Earth and Planetary Science Letters 286 (2009) 316–323

Contents lists available at ScienceDirect

Earth and Planetary Science Letters

journal homepage: www.elsevier.com/locate/epsl

Numerical simulation of atmospheric and oceanic biogeochemical cycles to an episodic CO_2 release event: Implications for the cause of mid-Cretaceous Ocean Anoxic Event-1a

Kazuhiro Misumi [a,b,*], Yasuhiro Yamanaka [a], Eiichi Tajika [c]

[a] Graduate School of Earth Environmental Science, Hokkaido University, N10 W5, Sapporo, Hokkaido 060-0810, Japan
[b] Environmental Science Research Laboratory, Central Research Institute of Electric Power Industry, 1646 Abiko, Abiko-shi, Chiba-ken 270-1194, Japan
[c] Graduate School of Science, The University of Tokyo, 7-3-1 Hongo, Bunkyo-ku, Tokyo 113-0033, Japan

ARTICLE INFO

Article history:
Received 15 October 2008
Received in revised form 25 June 2009
Accepted 28 June 2009
Available online 29 July 2009

Editor: M.L. Delaney

Keywords:
mid-Cretaceous
Ocean Anoxic Event
Ontong Java Plateau
numerical simulation

ABSTRACT

Response of biogeochemical cycles in the atmosphere and ocean to a major episode of CO_2 release event was investigated using numerical simulations. The results are applied to examine a previously proposed scenario for the Ocean Anoxic Event-1a (OAE-1a) caused by an episodic CO_2 release due to the Ontong Java Plateau (OJP) formation in the mid-Cretaceous. We developed an atmosphere–ocean biogeochemical cycle model that includes geochemical input to and output from the atmosphere and ocean due to submarine volcanic activity, continental weathering and sedimentation. We made a reference state, and then the state was perturbed in 42 cases of episodic CO_2 release with different rates and periods. In all cases, the elevated atmospheric CO_2 level results in an increase in phosphate concentration in the ocean caused by intensified weathering. Variations in the marine carbon isotope ratio are characterized by negative-to-positive excursions with a longer timescale for the latter. The deep water becomes anoxic in the cases with the release of a large amount of CO_2. These features are also seen in the geological records of OAE-1a. From quantitative comparisons, we found that the amount of CO_2 release required to cause OAE-1a is about 8×10^{18} mol, and atmospheric CO_2 increases by a factor of three or more (>3600 ppm) in these cases. The amount can be accounted for by CO_2 released due to the OJP formation, if the original magma contained a large CO_2 fraction. Therefore, we conclude that the OJP formation possibly caused OAE-1a.

1. Introduction

Sedimentary rocks formed in the mid-Cretaceous (Barremian to Turonian; 130.0–89.3 Ma; Gradstein et al., 2004) sporadically contain black shales rich in organic carbon. Since organic carbon hardly remains in seafloor sediments under oxic conditions, the formation of black shale is regarded as evidence for anoxic conditions in deep water. The deposition of black shale is limited to relatively short periods (10^5–10^6 yr), and thus the events are regarded as episodic (e.g., Leckie et al., 2002). The depositional events are termed "Ocean Anoxic Events (OAEs)" (Schlanger and Jenkyns, 1976), and five OAEs have been identified in the mid-Cretaceous (called OAE-1a to -1d, and OAE-2; e.g., Leckie et al., 2002; Erba, 2004).

The early Aptian OAE-1a is one of the most prominent OAEs both on temporal and spatial scales. In this event, anoxic conditions continue at least for 1×10^6 yr (Erba, 2004). Recent studies have revealed various environmental changes around this period, suggesting a causal relationship with OAE-1a. From radiometric and biostratigraphic ages, Larson and Erba (1999) suggested that the Ontong Java Plateau (OJP) formation began slightly before OAE-1a. The eruption of OJP likely occurred over a period shorter than 3×10^6 yr (Tarduno et al., 1991). Erba and Tremolada (2004) argued that the atmospheric CO_2 concentration increased by a factor of three to six during this event. Moreover, some studies have reported that the ocean was in eutrophic conditions during the period of OAE-1a (Bralower et al., 1994, 1999; Premoli Silva et al., 1999; Price, 2003; Erba, 1994, 2004).

At the timing of OAE-1a, large variations in the carbon isotope ratio ($\delta^{13}C$ values) of marine carbonate and organic carbon are recorded in numerous localities: e.g., Peregrina and Santa Rosa Canyons in Mexico (Scholle and Arthur, 1980; Bralower et al., 1999), Roter Sattel in Switzerland (Menegatti et al., 1998), Cismon in northern Italy (Menegatti et al., 1998; Erba et al., 1999), Vocontian Basin in southeastern France (Heimhofer et al., 2004), Paliambela in northwestern Greece (Danelian et al., 2004), ODP Site 866, DSDP Site 463 in the mid-Pacific mountains (Jenkyns and Strasser, 1995; Price, 2003), Cordillera Oriental in South America (Jahren et al., 2001). The $\delta^{13}C$ values show a short-term negative excursion followed by a long-term positive excursion (Fig. 1). Although the amplitudes of the negative-

* Corresponding author. Environmental Science Research Laboratory, Central Research Institute of Electric Power Industry, 1646 Abiko, Abiko-shi, Chiba-ken 270-1194, Japan. Tel.: +81 4 7182 1181; fax: +81 4 7183 2966.
E-mail address: misumi@criepi.denken.or.jp (K. Misumi).

0012-821X/$ – see front matter © 2009 Elsevier B.V. All rights reserved.
doi:10.1016/j.epsl.2009.06.045

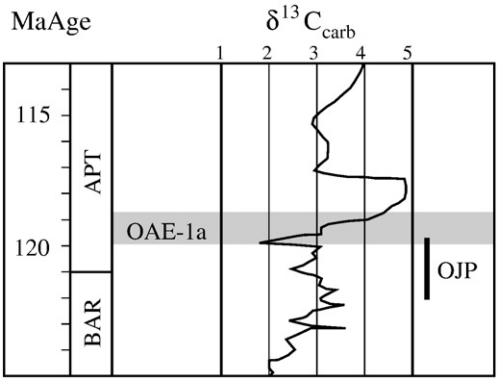

Fig. 1. Variations in carbon isotope ratio of marine carbonate across the OAE-1a modified from Erba (2004). Time-scale after Gradstein et al. (1995); $\delta^{13}C_{carb}$ curve after Erba et al. (1999) and Weissert et al. (1998); ages of Ontong Java Plateau (OJP) after Larson and Erba (1999).

to-positive excursions are different for each locality, with at least a 0.5‰ negative excursion followed by a 1.5‰ excursion are observed.

Larson and Erba (1999) proposed the following scenario accounting for the environmental changes and isotopic variations as mentioned above. The CO_2 release via volcanism due to mantle plume activity which formed the OJP led to a major climate warming. The warm climatic conditions induced intensified weathering and led to eutrophic ocean conditions. Export production increased and caused anoxic conditions in the deep water. The scenario also accounts for the variations of $\delta^{13}C$ values. Because carbon in the mantle has a low $\delta^{13}C$ value (about -5‰), abrupt CO_2 release due to the OJP formation should be recorded as a negative excursion of $\delta^{13}C$. As the ocean became eutrophic, productivity and organic matter burial increased, which is recorded as a positive excursion of $\delta^{13}C$. Thus an episodic CO_2 release event is recorded as a negative-to-positive excursion of $\delta^{13}C$. Kump and Arthur (1999) discussed the response of $\delta^{13}C$ to volcanic CO_2 release. However, their experiment did not consider the combined process that warm climatic conditions induced by volcanic CO_2 input intensified alkalinity and nutrient supply (e.g., phosphate) to the ocean. Moreover, they did not directly evaluate the scenario for the OJP formation as a cause of OAE-1a.

More recently, some studies indicated that the preceding negative excursion is very large (up to 4‰), and suggested a causal relationship with a massive release of ^{13}C depleted carbon either from a dissociation of CH_4 clathrate hydrates or from thermal metamorphism of C_{org}-rich sediments (Jahren et al., 2001; van Breugel et al., 2007; Ando et al., 2008). Li et al. (2008) argued that the negative shift occurred in a short period ($2.7–4.4\times10^4$ yr) using orbital chronology. Jahren et al. (2001) demonstrated that such a large and rapid negative excursion cannot be accounted for by CO_2 input due to volcanic activity, and concluded that a dissociation of CH_4 clathrate hydrates is the most reasonable cause for the negative excursion.

The purpose of this study is to examine the previously proposed scenario quantitatively with numerical simulations. In Section 2, we describe the model and experimental procedure. In Section 3, we show the results of responses of biogeochemical cycles in the atmosphere and ocean to episodic CO_2 release. In Section 4, we quantitatively evaluate the scenario, and summarize the results in Section 5.

2. Model

We developed a new model named "Mini earth system model for Million-year scale Climate change (MiMiC)". MiMiC is an atmosphere–ocean biogeochemical cycle model which includes geochemical fluxes of input to and output from the atmosphere and ocean by volcanic activity, continental weathering and sedimentation on the seafloor. We made a reference state of the system with MiMiC. Then the reference state was perturbed in 42 cases of CO_2 release with different rates and durations. Based on the results, we quantitatively discuss the causal relationship between the OJP formation and OAE-1a.

2.1. Biogeochemical cycles in the atmosphere and ocean

The atmosphere–ocean part of MiMiC is schematically drawn in Fig. 2. The area is horizontally divided into high and low latitude regions at the areal ratio of 1 to 25. The ocean is configured of 17 layers in the vertical direction. The layer thickness varies from 50 m for the top level to 350 m for the deepest level. The processes considered in the ocean part are the thermohaline circulation, and horizontal and vertical diffusions. Convective mixing process is considered at the high latitude regions. In the atmosphere part, the surface air temperatures are estimated from atmospheric CO_2 concentration determined from the biogeochemical part of the model. Detailed formulation for the atmosphere–ocean part is given in Appendix A. The biogeochemical part used in MiMiC is described in Yamanaka and Tajika (1996). The prognostic variables are phosphate, dissolved oxygen, total carbon, atmospheric CO_2 concentration, alkalinity and carbon isotope.

2.2. Processes of input to and output from the atmosphere and ocean

MiMiC includes geochemical fluxes of input to and output from the atmosphere and ocean due to volcanic activity, continental weathering and sedimentation on the seafloor. These processes are combined with the biogeochemical cycles in the atmosphere and ocean. The input and output processes are schematically drawn in Fig. 3.

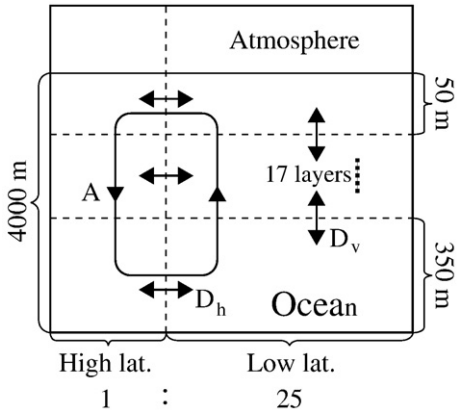

Fig. 2. Schematic structure of atmosphere–ocean part of MiMiC. Symbol "A" denotes advection by thermohaline circulation. Symbols of "D_h" and "D_v" denote horizontal and vertical diffusions. Detailed formulation and coefficients are described in Appendix A.

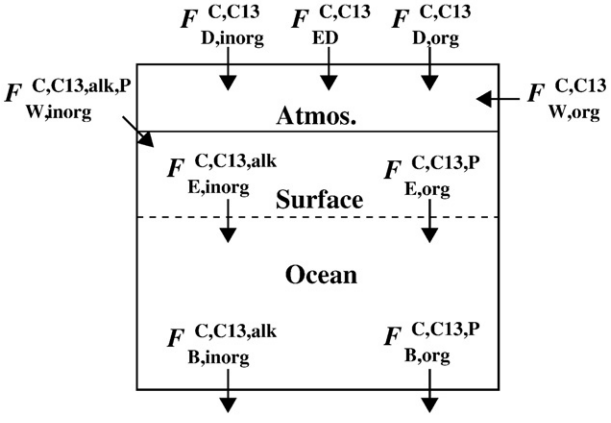

Fig. 3. Geochemical fluxes into and out of the atmosphere–ocean system. See text for the symbols.

We consider carbon and carbon isotope input fluxes to the atmosphere due to metamorphic/volcanic breakdown of carbonates ($F^{C}_{D,inorg}$, $F^{C13}_{D,inorg}$) and organic matter ($F^{C}_{D,org}$ and $F^{C13}_{D,org}$; Fig. 3). We also consider carbon and carbon isotope input fluxes to the atmosphere by an episodic volcanic event which releases a large amount of mantle derived CO_2 (F^{C}_{ED} and F^{C13}_{ED}; Fig. 3). Since we focus here on the influence of episodic volcanic events, we assume background volcanic CO_2 input from the mantle at mid-ocean ridges to be included in the fluxes due to metamorphic/volcanic breakdown of carbonates and organic matter. We also assume that $F^{C}_{D,inorg}$ and $F^{C}_{D,org}$ are constant in time, that is, $F^{C}_{D,inorg} = F^{C*}_{D,inorg}$ and $F^{C}_{D,org} = F^{C*}_{D,org}$ where superscript * represents constant (Table 1). The input rates of carbon isotope of $F^{C13}_{D,inorg}$ and $F^{C13}_{D,org}$ are defined here as $F^{C13}_{D,inorg} = \delta^{*}_{carb} F^{C*}_{D,inorg}$ and $F^{C13}_{D,org} = \delta^{*}_{org} F^{C*}_{D,org}$, where δ^{*}_{carb} and δ^{*}_{org} are carbon isotope ratios for carbonates and organic matter. We assume δ^{*}_{carb} and δ^{*}_{org} are constant (Table 1).

Weathering rates of carbonate and organic matter are represented by $F_{W,inorg}$ and $F_{W,org}$ (Fig. 3) $F^{C}_{W,inorg}$, $F^{C13}_{W,inorg}$, $F^{alk}_{W,inorg}$ and $F^{P}_{W,inorg}$ represent carbon, carbon isotope, alkalinity and phosphate input fluxes due to weathering, respectively. The input rates vary owing to changes in paleogeography, soil biological activity, reservoir sizes and atmospheric CO_2 concentration (Berner, 1991), however, in the timescale discussed here (about 10^6 yr), the changes in the input rates are caused mainly by the change in atmospheric CO_2 concentration. We therefore only consider the effect of atmospheric CO_2 partial pressure, which is represented as a dimensionless feedback function of $f(CO_2)$. Thus we assume the relationship of $F^{C}_{W,inorg} = f(CO_2) F^{C*}_{W,inorg}$, $F^{C13}_{W,inorg} = f(CO_2)\delta^{*}_{carb} F^{C*}_{W,inorg}$, $F^{alk}_{W,inorg} = f(CO_2) F^{alk*}_{W,inorg}$ and $F^{P}_{W,inorg} = f(CO_2) F^{P*}_{W,inorg}$. For simplicity, we assume a single function that Berner (1994) used for silicate mineral,

$$f(CO_2) = \exp(0.09 \times \Delta T) \times (1 + 0.038 \times \Delta T)^{0.065} \times \{2 \times RCO_2 / ((1 + RCO_2))\}^{0.4}, \quad (1)$$

where ΔT is the deviation of globally averaged surface temperature from the present, RCO_2 is the ratio of atmospheric CO_2 concentration to that at present (300 ppm). We assume $F^{C*}_{W,inorg}$ to be the value at present (Berner, 1991; Table 1). $F^{alk*}_{W,inorg}$ and $F^{P*}_{W,inorg}$ are determined from alkalinity and phosphate balance of the ocean in the reference state as will be described later. $F^{C}_{W,org}$ and $F^{C13}_{W,org}$ represent carbon and carbon isotope input fluxes due to oxidative weathering of organic matter, respectively. The input rates vary owing to changes in paleogeography and mean land elevation (Berner, 1991). We assume these fluxes to be constant in this study (Table 1).

Sedimentation rates of carbonate and organic matter are represented by $F_{B,inorg}$ and $F_{B,org}$ (Fig. 3). $F^{C}_{B,inorg}$, $F^{C13}_{B,inorg}$ and $F^{alk}_{B,inorg}$ represent carbon, carbon isotope and alkalinity output rates due to carbonate precipitation, respectively. $F^{C}_{B,org}$, $F^{C13}_{B,org}$ and $F^{P}_{B,org}$ represent carbon, carbon isotope and phosphate output rates due to burial of organic matter, respectively. The sedimentation rates would be proportional to export production ($F_{E,inorg}$ and $F_{E,org}$) at the bottom of the surface water (Fig. 3). We assume $F_{B,inorg} = B_{inorg} F_{E,inorg}$ and $F_{B,org} = B_{org} F_{E,org}$, where B_{inorg} and B_{org} are burial efficiencies of carbonate and organic matter. Although the burial efficiencies might vary owing to changes in ocean environments, we assume the burial efficiencies as constant in time, that is $F^{C}_{B,inorg} = B^{*}_{inorg} F^{C}_{E,inorg}$, $F^{C13}_{B,inorg} = B^{*}_{inorg} \delta_{exp} F^{C}_{E,inorg}$, $F^{alk}_{B,inorg} = B^{*}_{inorg} F^{alk}_{E,inorg}$, $F^{C}_{B,org} = B^{*}_{org} F^{C}_{E,org}$, $F^{C13}_{B,org} = B^{*}_{org} (\delta_{exp} - \alpha^{*}) F^{C}_{E,org}$ and $F^{P}_{B,org} = B^{*}_{org} F^{P}_{E,org}$ where δ_{exp} is the carbon isotope ratio of carbonate determined from the $\delta^{13}C$ value of the surface ocean and α^{*} is the carbon isotopic fractionation due to photosynthesis (Table 1). We use constant α^{*}, for simplicity.

In the biogeochemical part of MiMiC, we assume $F^{P}_{E,org}$ to be proportional to phosphate concentration in the surface water, and $F^{P}_{E,org}$ to be combined with the other export fluxes of $F^{C}_{E,org}$, $F^{C}_{E,inorg}$, $F^{alk}_{E,inorg}$, $F^{C13}_{E,inorg}$ and $F^{C13}_{E,org}$ as follows: $F^{C}_{E,org} = R^{*} F^{P}_{E,org}$, $F^{C}_{E,inorg} = r^{*} F^{C}_{E,org}$, $F^{alk}_{E,inorg} = 2F^{C}_{E,inorg}$, $F^{C13}_{E,inorg} = \delta_{exp} F^{C}_{E,inorg}$ and $F^{C13}_{E,org} = (\delta_{exp} - \alpha^{*}) F^{C}_{E,org}$, where R^{*} is the Redfield ratio, and r^{*} is the rain ratio. We use constant values for R^{*} and r^{*}, for simplicity (Table 1). Thus all the burial fluxes are finally proportional to phosphate concentration in the surface water in this model.

The burial efficiencies of B^{*}_{inorg} and B^{*}_{org} are determined from the carbon and carbon isotope mass balance for the atmosphere–ocean system in the reference state, which is described as

$$F^{C*}_{D,inorg} + f(CO_2) F^{C*}_{W,inorg} + F^{C*}_{D,org} + F^{C*}_{W,org} = B^{*}_{inorg} F^{C}_{E,inorg} + B^{*}_{org} F^{C}_{E,org}, \quad (2)$$

$$F^{C13*}_{D,inorg} + f(CO_2) F^{C13*}_{W,inorg} + F^{C13*}_{D,org} + F^{C13*}_{W,org} = B^{*}_{inorg} F^{C13}_{E,inorg} + B^{*}_{org} F^{C13}_{E,org}. \quad (3)$$

Giving the atmospheric CO_2 in the reference state, all the values on the left-hand side are given (Table 1). The export production of $F_{E,inorg}$ and $F_{E,org}$ on the right-hand side are independently determined from Eqs. (2) and (3), by calculating the model with the atmospheric CO_2 concentration in the reference state and assuming a "closed system" where no geochemical input to and output from the atmosphere and ocean system is considered. Assuming the obtained values of $F_{E,inorg}$ and $F_{E,org}$ in Eqs. (2) and (3), we can determine B^{*}_{inorg} and B^{*}_{org} (Table 1). $F^{alk*}_{W,inorg}$ and $F^{P*}_{W,inorg}$ are determined from the mass balance of the alkalinity and phosphate in the ocean in the reference state:

$$f(CO_2) F^{alk*}_{W,inorg} = B^{*}_{inorg} F^{alk}_{E,inorg}, \quad (4)$$

$$f(CO_2) F^{P*}_{W,inorg} = B^{*}_{org} F^{P}_{E,org}. \quad (5)$$

The same burial efficiencies determined in the previous step are used for these equations. The export fluxes of $F^{alk}_{E,inorg}$ and $F^{P}_{E,org}$ are also estimated by calculating the model with the atmospheric CO_2

Table 1
Constants used in our experiment.

Symbol	Meaning	Value	Reference
$F^{C*}_{D,inorg}$	CO_2 input rates due to metamorphic/volcanic breakdown of carbonates	6.65 Tmol/yr	Berner (1991)
$F^{C*}_{D,org}$	CO_2 input rates due to metamorphic/volcanic breakdown of organic matter	1.25 Tmol/yr	Berner (1991)
$F^{C*}_{W,inorg}$	Carbon input rates due to weathering of minerals	13.35 Tmol/yr	Berner (1991)
$F^{C*}_{W,org}$	CO_2 input rates due to weathering of organic matter	3.75 Tmol/yr	Berner (1991)
$F^{alk*}_{W,inorg}$	Alkalinity input rates due to weathering of minerals	29.6 Teq/yr	This study
$F^{P*}_{W,inorg}$	Phosphate input rates due to weathering of minerals	0.044 Tmol/yr	This study
B^{*}_{inorg}	Burial coefficient for calcite	0.30	This study
B^{*}_{org}	Burial coefficient for organic matter	0.0077	This study
δ^{*}_{carb}	Carbon isotope ratio for carbonate	1.5‰	Berner (1991)
δ^{*}_{org}	Carbon isotope ratio for organic matter	−23.5‰	Berner (1991)
α^{*}	Isotopic fractionation by organisms	25.0‰	Berner (1991)
R^{*}	Redfield ratio for P:C	106	Redfield et al. (1963)
r^{*}	Rain ratio	0.08	Yamanaka and Tajika (1996)

concentration in the reference state and assuming a "closed system". Then, we can obtain $F^{alk*}_{W,inorg}$ and $F^{P*}_{W,org}$ by solving Eqs. (4) and (5) (Table 1).

2.3. Procedure

The reference state is obtained by conducting the following two preliminary experiments. We chose the atmospheric CO_2 concentration of 1200 ppm for the reference state, referring to the early Aptian CO_2 level (Tajika, 1998, 1999; Heimhofer et al., 2004). We calculate MiMiC under the "closed system" with a fixed atmospheric CO_2 concentration of 1200 ppm and an atmospheric carbon isotope ratio of −3‰ (e.g., Gröcke, 2002). Sea surface temperatures in high and low latitudes are restored to estimated temperatures calculated in the atmosphere part (see Appendix A). Sea surface salinities in high and low latitudes are restored to 33 and 35 psu, respectively. In this calculation, the obtained steady state is independent of the initial conditions for temperature, salinity, dissolved oxygen, total carbon concentrations and carbon isotope in the ocean. On the other hand, initial conditions for phosphate and alkalinity are not constrained in this model. We arbitrarily chose these values four times higher than present values. We calculated for 3×10^5 yr under the conditions, and obtained a steady state. Then, we calculated MiMiC under an "open system" condition by solving the mass balance equations of Eqs. (2)–(5) and determining the constants of B^*_{inorg}, B^*_{org}, $F^{alk*}_{W,inorg}$ and $F^{P*}_{W,inorg}$. We calculated for 2.7×10^6 yr, and obtained values of B^*_{inorg}, B^*_{org}, $F^{alk*}_{W,inorg}$ and $F^{P*}_{W,org}$ are shown in Table 1. The steady state is used as the reference state.

The reference state was perturbed by 42 cases of episodic CO_2 release via volcanism with different CO_2 input rates (F_{ED}) and durations (Fig. 4). We chose the maximum duration as 3×10^6 yr according to Tarduno et al. (1991). We assume $\delta^{13}C$ of −5‰ for F_{ED}. In all the cases, the simulations start from -1×10^5 yr, and the additional CO_2 input starts at 0 yr. The calculations continue until a steady state is achieved after the perturbation.

3. Results

We show the results of time variations of model variables for a standard case. Then, we summarize the responses of $\delta^{13}C_{carb}$ values and oxygen concentration in the deep ocean for all the cases.

3.1. A standard case

As a standard case, we show the results of time variations of the model variables for the case with the additional CO_2 input rate of 20 Tmol/yr and duration of 1×10^6 yr (Fig. 5; corresponding to the case indicated by an arrow in Fig. 4). The additional CO_2 release brings the atmospheric CO_2 concentration to about 8500 ppm which is seven times higher than that in the reference state (Fig. 5b). The warm climatic condition increases the phosphate concentration to 30 μmol/L owing to intensified weathering (Fig. 5c). The deep water becomes anoxic (Fig. 5d) owing to the combination of decreased oxygen solubility in the deep water formation area due to the increase in sea surface temperature (not shown) and increased bioproductivity due to increased phosphate concentration (Fig. 5c). The anoxic condition continues for about 1.5×10^6 yr (Fig. 5d). After the episodic CO_2 release ceased, biogeochemical cycles return to the reference state.

The variation of $\delta^{13}C_{carb}$ deviation from the reference value ($\Delta\delta^{13}C_{carb}$) shows a short-term negative excursion followed by a long-term positive excursion (Fig. 5e). The negative excursion is caused by mantle derived CO_2 input with low $\delta^{13}C$. The positive excursion occurs with two steps. The first step begins at about 1×10^5 yr and continues until the end of the CO_2 release (1×10^6 yr). This increase is caused by the removal of isotopically light carbon due to the increased burial flux of organic carbon. Intensified weathering under the high atmospheric CO_2 condition (Fig. 5b) increases phosphate concentration and export production in the ocean, resulting in an increase in the burial flux of organic carbon. The second step begins after the end of the CO_2 release (1×10^6 yr). Since the mantle derived CO_2 input suppressed increase in the $\delta^{13}C_{carb}$ value during the eruption period, the cessation of CO_2 input under high phosphate concentration causes further increase in the $\delta^{13}C_{carb}$ value. The $\delta^{13}C_{carb}$ value returns to the reference state as the phosphate concentration decreases to the reference value. In this case, the $\Delta\delta^{13}C_{carb}$ value decreases by −1.5‰, and, then, increases by 2.5‰.

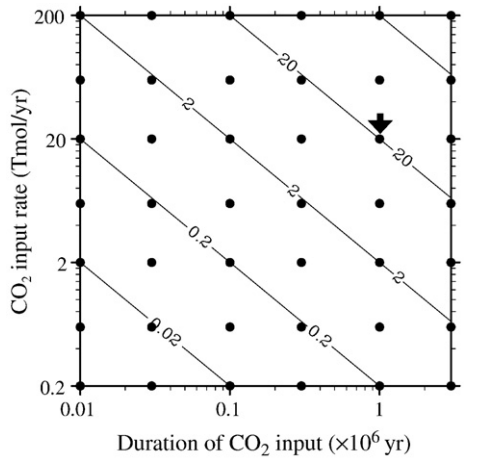

Fig. 4. Summary of the results for all cases. The condition for each case is represented as a black dot. Note that both axes are drawn on a log-scale. The total amount of CO_2 input is a product of the input rate and the duration, and is constant along the contour line (called isoamount lines). The case represented by a downward arrow is shown in Fig. 5.

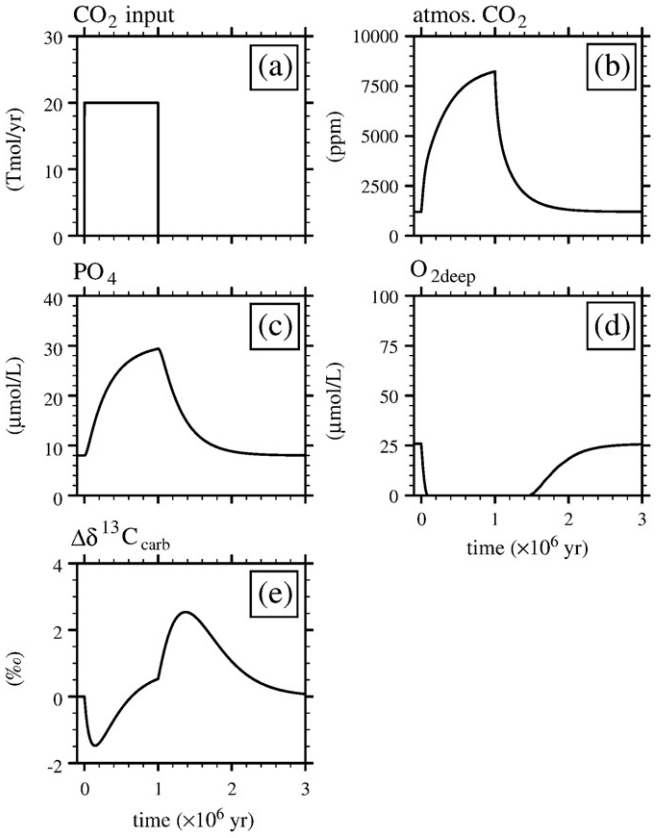

Fig. 5. The results of the case with the CO_2 release rate of 20 Tmol/yr and the duration of 1×10^6 yr. Time variations of (a) episodic CO_2 release, (b) atmospheric CO_2 concentration, (c) mean phosphate concentration in the ocean, (d) oxygen concentration in the deep water, (e) the deviation of carbon isotopic composition of carbonate precipitated in the surface water from the reference value ($\Delta\delta^{13}C_{carb}$).

Although the amplitudes and durations of the negative–positive excursions are different in each case, the negative-to-positive excursion is a common characteristic feature for all the cases.

The rates of increases in atmospheric CO_2, phosphate concentrations, and $\delta^{13}C_{carb}$ value are suppressed during the CO_2 release (Fig. 5b, c, e). This is because a negative feedback as suggested by Walker et al. (1981) operates. The feedback is simulated in MiMiC as follows: the increase in atmospheric CO_2 concentration intensifies weathering fluxes of $F^{alk}_{W,inorg}$ and $F^{P}_{W,inorg}$, which increase ocean alkalinity and phosphate concentration. The higher alkalinity decreases ocean pCO_2 and promotes CO_2 absorption from the atmosphere, which declines the rates of increase in atmospheric CO_2 concentration (Fig. 5b). The increase in phosphate concentration intensifies burial fluxes of $F_{B,org}$ and $F_{B,inorg}$, which decreases the rate of increase in phosphate concentration (Fig. 5c). Finally, biogeochemical cycles reach another steady state where the mantle derived CO_2 input balances with the intensified carbon output. In fact, atmospheric CO_2, phosphate concentrations, and the $\delta^{13}C$ value reach steady state levels in the case with the CO_2 release duration of 3×10^6 yr (not shown).

3.2. Summary of all results

The maximum deviation of $\delta^{13}C_{carb}$ values during the negative excursion from the reference state (we call this a negative deviation or negative $\Delta\delta^{13}C_{carb}$) tends to increase as the amount of CO_2 input becomes large (Fig. 6a). This proportionality can be found in the contour lines that are almost parallel to the isoamount lines (Fig. 4) in the cases with the duration shorter than 1×10^5 yr. On the other hand, the lines are almost parallel to the horizontal axis in the cases with the duration longer than 1×10^5 yr. This implies that the negative deviations are not sensitive to the duration of CO_2 input. This is because the $\delta^{13}C_{carb}$ value starts to increase after the CO_2 input continues for longer than 1×10^5 yr (Fig. 5e). It is also important to note that the negative deviations cannot exceed 4‰ even in the cases with large CO_2 input rates.

The maximum deviation of $\delta^{13}C_{carb}$ values during the positive excursion from the reference state (hereafter, we call this a positive deviation, or positive $\Delta\delta^{13}C_{carb}$) also increase as the amount of CO_2 input becomes large, but the timescale being insensitive to the duration of CO_2 input is longer than that in the negative one (Fig. 6b). Since biogeochemical cycles reach another steady state after the CO_2 input continues for longer than 1×10^6 yr, the positive deviations are not sensitive to the duration of CO_2 input. The positive deviations become over 5‰ in the cases with a large CO_2 input.

In the cases with a large amount of CO_2 input, the deep water becomes anoxic (<10 μmol/L) (Fig. 6c). It is interesting to note that the durations of anoxic conditions are not simply proportional to the duration of CO_2 input (Fig. 6d). In most cases, the durations are longer than the duration of CO_2 input. This is because the elevated phosphate concentration keeps the deep water anoxic until the phosphate concentration decreases enough after the CO_2 input stops (Fig. 5c, d).

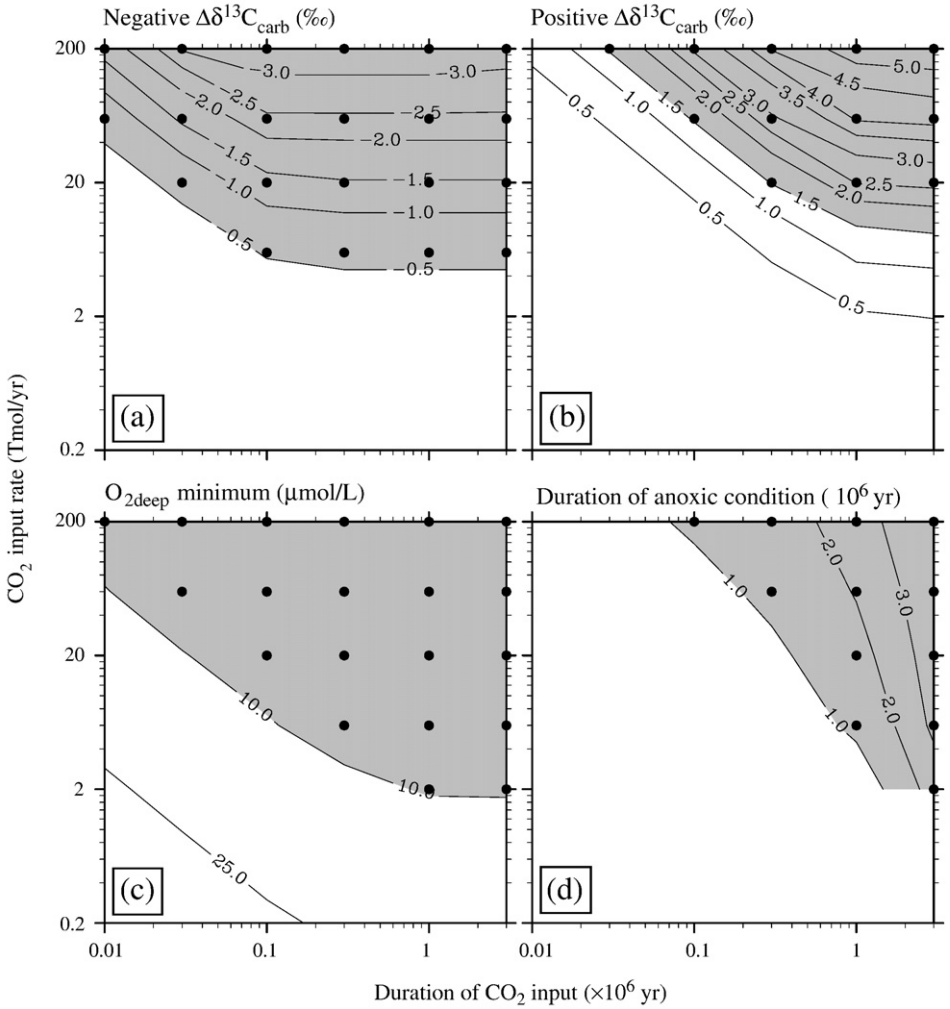

Fig. 6. (a) The maximum deviation of $\delta^{13}C_{carb}$ during the negative excursion for all the cases. (b) The maximum deviation of $\delta^{13}C_{carb}$ during the positive excursion for all the cases. (c) The minimum values of oxygen concentration in the deep water. (d) The duration of anoxic condition in the deep water. Black dots and shade indicate the cases and region which satisfy the constraint for the observed negative and positive excursions, oxygen concentration, duration of anoxic condition, respectively (see the text).

4. Discussion

The results of the numerical simulations indicate that atmospheric CO_2 and ocean phosphate concentrations increase owing to an additional CO_2 input via plume-derived volcanism. The response of $\delta^{13}C_{carb}$ values is characterized by a short-term negative excursion followed by a long-term positive excursion. The deep water becomes anoxic when the additional CO_2 input is very large. In this section, we compare the results with the geological record of OAE-1a. We evaluate the amount of CO_2 input required for explaining the observed variations of $\delta^{13}C$ during OAE-1a. Then we discuss the possibility that the estimated amount of CO_2 was released by the OJP formation. Finally, we discuss the effects of changes in biogeochemical cycles under anoxic conditions on our results.

Carbon isotope record of OAE-1a is characterized by a short-term negative excursion followed by a long-term positive excursion. The simulated results qualitatively capture this characteristic feature (Fig. 5e), suggesting that the OJP formation could be a candidate for the cause of OAE-1a. Here, we introduce three constraints for the environmental changes during OAE-1a. The first constraint is for negative $\Delta\delta^{13}C$, that is, the maximum deviation of $\delta^{13}C$ in the negative excursion. Geological record of OAE-1a shows that the negative $\Delta\delta^{13}C$ value exceeds, at least, 0.5‰ (Scholle and Arthur, 1980; Jenkyns and Strasser, 1995; Menegatti et al., 1998; Price, 2003; Danelian et al., 2004). The second constraint is for positive $\Delta\delta^{13}C$, that is, the maximum deviation of $\delta^{13}C$ in the positive excursion. Geological record of OAE-1a shows that the positive $\Delta\delta^{13}C$ value exceeds, at least, 1.5‰ (Jenkyns and Strasser, 1995; Menegatti et al., 1998; Weissert et al., 1998; Bralower et al., 1999; Price, 2003; Danelian et al., 2004). The last constraint is for the oxygen concentration in the deep water. Geological record of OAE-1a suggests that deep water became anoxic, and this condition continued for, at least, 1×10^6 yr (Erba, 2004). The cases and region which satisfy these constraints are shown as black dots and shade in Fig. 6.

A composite of the constraints gives an estimation of the required amount of CO_2 causing OAE-1a (Fig. 7). Upper right part of the region, that is the most heavily shaded region with a dashed line, satisfies all the constraints. In the cases with the duration of CO_2 input shorter than 0.5×10^6 yr, the dashed line is roughly parallel to the isoamount lines (Fig. 4), meaning that the minimum amount of CO_2 release required for explaining the environmental changes during OAE-1a is approximately constant, and is about 8×10^{18} mol (=8 Emol; e.g., 0.4×10^6 yr × 20 Tmol/yr). In the cases with the duration of CO_2 input longer than 0.5×10^6 yr, the minimum amount increases as the duration of CO_2 input elongates. Thus, if the OJP formation released 8 Emol or more CO_2 to the atmosphere–ocean system, the scenario that the OJP formation caused OAE-1a is quantitatively supported.

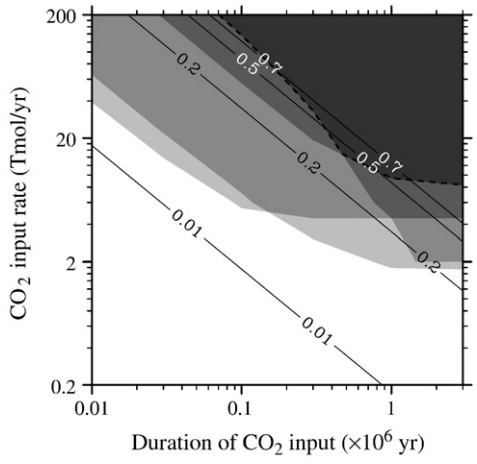

Fig. 7. Composite of the results which satisfy the individual constraints. The most heavily shaded region with a dashed line satisfies all the constraints. Lines indicate the estimated amount of CO_2 release via the OJP formation with weight fraction of original magma of 0.01, 0.2, 0.5 and 0.7 wt.%, respectively.

Is it possible for the OJP formation to have released more than 8 Emol of CO_2 to the atmosphere–ocean system? Here, we estimate the CO_2 amount released by the OJP formation. According to Leavitt (1982), the number of moles of CO_2 released during a volcanic eruption is estimated as follows:

$$mCO_2 = s \times dg \times v \times d / m.w.CO_2 \quad (6)$$

where s is the weight fraction of CO_2 in the magma, dg is the degassing fraction during the eruption, v is the magma volume, d is the solid density of the magma and m.w.CO_2 is the molecular weight of CO_2 (44 g). For typical basaltic lavas, the values for dg and d are 0.6 and 2.9 g/cm^3, respectively (Leavitt, 1982). The volume of OJP is estimated as 4.4×10^7 km^3 (Eldholm and Coffin, 2000).

The remaining parameter of the weight fraction of CO_2 is the most difficult to determine because erupted melt does not retain the original CO_2 content. Most of CO_2 contained in the melt is released as it approaches to the earth surface, however there is no way of knowing how extensively the melt degassed. Indeed, we do not know whether the original melt was undersaturated, saturated or oversaturated with CO_2, and how largely gaseous CO_2 co-occurred. Therefore, estimations of the weight fraction of CO_2 could vary more than an order of magnitude, and the value of the OJP eruption has not been fully clarified.

In this study, we use four estimations of s, that is 0.01, 0.2, 0.5 and 0.7 wt.%, respectively. The first estimation is derived from the mid-ocean-ridge basalt (Saal et al., 2002), and the second one is derived from averaging values of experimental CO_2 solubility and the measurement of CO_2 in the deep-sea basalt (Leavitt, 1982). The latter two estimations are derived from observations in Kilauea volcano (Gerlach and Graeber, 1985; Gerlach et al., 2002). Since the OJP eruption is presumed to be plume-derived volcanism, preferred estimate may be the latter two estimations. The estimated CO_2 amounts released by the OJP formation are 0.17, 3.5, 8.7 and 12 Emol, respectively (the isoamount lines are shown in Fig. 7). Because the lines with 0.5 and 0.7 wt.% overlap the region satisfying all the constraints, the episodic CO_2 release due to the OJP formation can quantitatively cause the environmental variation observed during OAE-1a, although a large fraction of CO_2 is required for the original magma. In addition, our results confirm an estimation of CO_2 increase at the time of OAE-1a. In the cases satisfying all the constraints, atmospheric CO_2 increases three times or more (>3600 ppm) compared with the pre-OAE-1a condition (not shown). Erba and Tremolada (2004) estimated an increase of CO_2 of three to six times, which corresponds to lower part of our results.

Although we have assumed the constraint for negative excursion as 0.5‰, some studies have reported a larger negative excursion (up to 4‰) at the onset of OAE-1a (Jahren et al. 2001; van Breugel et al., 2007; Ando et al., 2008). Our results ascertain that such a large negative excursion cannot be accounted for only by CO_2 input due to a volcanic eruption, even though the input rate is extremely large (Fig. 6a). Therefore, if the large negative excursion represents a perturbation of the global carbon cycle, we concur with the suggestion that a dissociation of CH_4 clathrate hydrates is the main cause for the negative excursion. On the other hand, our results suggest that the positive excursion and deep-water anoxia over 1.0×10^6 yr cannot be accounted for by a dissociation of CH_4 clathrate hydrates. These are caused by global warming, and the required amount of CO_2 input is over 8.0×10^{18} mol (Fig. 7). Since CH_4 is rapidly oxidized in the atmosphere and ocean (about 10 yr), the long-term radiative forcing effect is comparable to that of CO_2. For this reason, the same order of magnitude of CH_4 release is required to account for causing the positive excursion and deep-water anoxia. The amount is over an order of magnitude higher than an estimated amount of CH_4 clathrate hydrates at present (2.5×10^{17} mol; Buffett and Archer, 2004).

Therefore we conclude that the main driver causing OAE-1a will be the OJP formation, though a dissociation of CH_4 clathrate hydrates likely contributes to cause the negative excursion.

We have assumed constant burial efficiencies for inorganic and organic matter, but the efficiencies likely change during the anoxic event. Sedimentary rocks at the timing of OAE-1a show increased organic carbon and decreased carbonate contents (i.e., van Breugel et al., 2007), which means increased and decreased burial efficiencies of organic carbon and calcium carbonate, respectively. Furthermore, phosphorus will be preferentially released from sediment under anoxic conditions (i.e., Ingall and Jahnke, 1997), which suggests a decreased burial efficiency of phosphorus during the event. These biogeochemical changes may alter the model responses to volcanic CO_2 inputs. To examine the effects, we conducted experiments that double B_{org} for organic carbon and half B_{inorg} for calcium carbonate and phosphorus. Since decoupling of the alkalinity and phosphorus cycles is difficult due to the model formulations, we simultaneously decrease B_{inorg} for calcium carbonate and phosphorus. We perturb B_{org} and B_{inorg} during a period from 0.2×10^6 to 1.2×10^6 yr for the case described in Fig. 5.

In the case of doubled B_{org}, increase in removal of isotopically light carbon causes a larger positive excursion than that in the standard case (Fig. 8a). It is, however, important to note that the relative strength of the burial flux of organic carbon in the perturbed case to that in the standard case decreases with time (Fig. 8b). This is because the increased burial flux decreases the atmospheric CO_2 (Fig. 8c), phosphate supply to the ocean, and finally, export production in the ocean (Fig. 8d). As a result, the increase in burial efficiency finally decreases the burial flux of organic carbon. Without including the feedback process, we would overestimate the effects of increase in the burial efficiency of organic carbon.

In the case of half B_{inorg}, a larger positive excursion is also observed (Fig. 8a), although the mechanism is different from that in the previous case. The decreased phosphorus burial efficiency increases the phosphate concentration in the ocean, which intensifies the export production (Fig. 8d) and the burial flux of organic carbon (Fig. 8b). As a result, the $\delta^{13}C_{carb}$ value shows a larger positive excursion. In this case, atmospheric CO_2 decreases mainly because ocean alkalinity increases due to a decrease in precipitation of calcium carbonate.

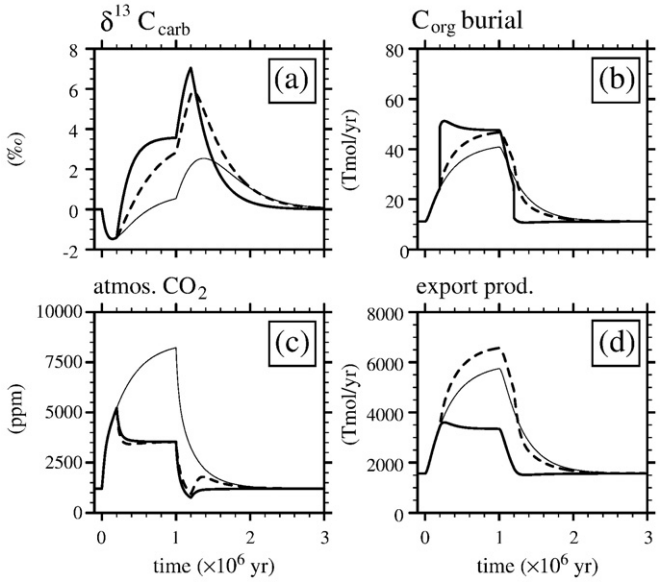

Fig. 8. The results of the case perturbing burial efficiencies during a period from 0.2×10^6 to 1.2×10^6 yr for the case CO_2 release rate of 20 Tmol/yr and the duration of 1×10^6 yr. Thin, bold and dotted lines indicate the results of the standard, doubled B^{C}_{org} and half $B^{P,\ alk}_{inorg}$, respectively. Time variations of (a) the deviation of carbon isotope composition of carbonate from the reference value, (b) burial flux of organic carbon, (c) atmospheric CO_2 concentration and (d) export production from the surface water.

In this way, the changes in sedimentary output fluxes under anoxic conditions tend to enlarge positive excursions and weaken the constraint for it. Therefore, if we fully implemented the changes in MiMiC, the required impact which can cause OAE-1a would decrease because the constraint enlarges it (Figs. 6b, 7). Quantitative information about the changes in sedimentary output fluxes during OAE-1a will provide a better constraint on the causal relationship between the OJP formation and OAE-1a.

5. Conclusion

We developed a model of the biogeochemical cycle in the atmosphere–ocean system which is named Mini earth system model for Million-year scale Climate change (MiMiC). Using MiMiC, we have numerically assessed the previously proposed scenario that the Ontong Java Plateau (OJP) formation caused OAE-1a. The obtained results are very similar to those observed in the geological record during OAE-1a. Moreover, the amount of CO_2 release required for explaining the environmental changes during OAE-1a (such as the carbon isotopic variations) is estimated to be, at least, 8×10^{18} mol. Assuming large weight fractions of CO_2 in the original magma as found for the Kilauea volcano, the required amount of CO_2 release can be explained by the OJP formation. In addition, the necessary weight fraction tends to decrease when we consider biogeochemical cycle changes under anoxic conditions. Therefore, we conclude that the OJP formation possibly caused OAE-1a.

Acknowledgments

We thank A. Abe-Ouchi, N. Ohkouchi, and J. Kuroda, for discussion and giving perceptive comments. This paper also benefited from insightful comments from R.M. Leckie, and an anonymous reviewer. One of the authors, K. Misumi, was supported by Central Research Institute of Electric Power Industry and the 21st century Center of Excellence Program funded by Ministry of Education, Culture, Sports, Science and Technology. All the figures were produced with the GFD-DENNOU Library.

Appendix A. Atmosphere and ocean part of MiMiC

The atmosphere–ocean part of MiMiC are described, see also Fig. 2. In the ocean part, distributions of temperature and concentrations of salinity and chemical tracers in the ocean are determined by solving the advection and diffusion equation of

$$\frac{\partial C}{\partial t} = \frac{\partial}{\partial z}\left(-wC + K_v\frac{\partial C}{\partial z}\right) + D(C), \tag{1}$$

where C represents the temperature and concentrations of salinity and chemical tracers, w is the vertical velocity by the thermohaline circulation, K_v is the vertical diffusion coefficient, and D represents horizontal mixing of the temperature and concentrations. The vertical velocity of w is determined as the mass flux is to 20×10^6 m^3/s that is the same order of magnitude as that in the present. Depth dependent vertical diffusion coefficients of Tsujino et al. (2000) are used for K_v, though the values in the surface water are slightly higher than those in the original (Table A.1). The horizontal mixing is parameterized as the following equations

$$D_{h,k}(C) = d_k\left(C_{l,k} - C_{h,k}\right) \tag{2}$$

$$D_{l,k}(C) = -\frac{D_{h,k}}{r}, \tag{3}$$

where the first subscript indicates high (h) or low (l) latitude grids and the second subscript means the vertical level, d is the horizontal

mixing coefficient, r is an areal ratio between high and low latitudes. We used larger values for d representing the strong wind-driven mixing for the surface water (Table A.1).

Surface air temperatures in the high and low latitudes are estimated from atmospheric CO_2 concentration using the following equation

$$T_l(CO_2) = 5.2 \times \log(CO_2) + 20.2 \quad (4)$$

$$T_h(CO_2) = 9.5 \times \log(CO_2) - 3.3. \quad (5)$$

We obtained these equations referring to the results of an coupled atmosphere–ocean model (Stouffer and Manabe, 2003).

Table A.1
Vertical and horizontal diffusion coefficients used in our model.

Depth (m)	K_v (m^2/s)	d_k (1/s)
25	0.50×10^{-4}	7.6×10^{-9}
75	0.50×10^{-4}	5.8×10^{-9}
135	0.50×10^{-4}	1.6×10^{-9}
210	0.50×10^{-4}	9.7×10^{-11}
300	0.50×10^{-4}	2.7×10^{-12}
425	0.50×10^{-4}	1.0×10^{-12}
575	0.50×10^{-4}	1.0×10^{-12}
750	0.50×10^{-4}	1.0×10^{-12}
975	0.50×10^{-4}	1.0×10^{-12}
1250	0.62×10^{-4}	1.0×10^{-12}
1550	0.99×10^{-4}	1.0×10^{-12}
1875	1.48×10^{-4}	1.0×10^{-12}
2225	2.01×10^{-4}	1.0×10^{-12}
2600	2.46×10^{-4}	1.0×10^{-12}
3000	2.74×10^{-4}	1.0×10^{-12}
3400	2.88×10^{-4}	1.0×10^{-12}
3800	2.95×10^{-4}	1.0×10^{-12}

References

Ando, A., Kaiho, K., Kawahata, H., Kakegawa, T., 2008. Timing and magnitude of early Aptian extreme warming: unraveling primary $\delta^{18}O$ variation in indurated pelagic carbonates at Deep Sea Drilling Project Site 463, central Pacific Ocean. Palaeogeogr. Palaeoclimatol. Palaeoecol. 260, 463–476.

Berner, R.A., 1991. A model for atmospheric CO_2 over Phanerozoic time. Am. J. Sci. 291, 339–376.

Berner, R.A., 1994. GEOCARB II: a revised model of atmospheric CO_2 over Phanerozoic time. Am. J. Sci. 294, 56–91.

Bralower, T.J., Arthur, M.A., Leckie, R.M., Sliter, W.V., Allard, D.J., Schlanger, S.O., 1994. Timing and paleoceanography of oceanic dysoxia/anoxia in the late Barremian to early Aptian (early Cretaceous). Palaios 9, 335–369.

Bralower, T.J., CoBabe, E., Clement, B., Sliter, W.V., Osburn, C.L., Longoria, J., 1999. The record of global change in mid-Cretaceous (Barremian–Albian) sections from the Sierra Madre, northeastern Mexico. J. Foraminiferal Res. 29, 418–437.

Buffett, B., Archer, D., 2004. Global inventory of methane clathrate: sensitivity to changes in the deep ocean. Earth Planet. Sci. Lett. 227, 185–199.

Danelian, T., Tsikos, H., Gardin, S., Baudin, F., Bellier, J.-P., Emmanuel, L., 2004. Global and regional palaeoceanographic changes as recorded in the mid-Cretaceous (Aptian–Albian) sequence of the Ionian zone (NW Greece). J. Geol. Soc. 161, 703–709.

Eldholm, O., Coffin, M.F., 2000. Large igneous provinces and plate tectonics. The History and Dynamics of Global Plate Motions: Geophys. Monogr., vol. 121, pp. 309–326.

Erba, E., 1994. Nannofossils and superplumes: the early Aptian "nannoconid crisis". Paleoceanography 9, 483–501.

Erba, E., Channell, J.E.T., Claps, M., Jones, C., Larson, R., Opdyke, B., Premoli Silva, I., Riva, A., Salvini, G., Torricelli, S., 1999. Integrated stratigraphy of the Cismon APTICORE (Southern Alps, Italy): a "Reference section" for the Barremian–Aptian interval at low latitudes. J. Foraminiferal Res. 29, 371–391.

Erba, E., 2004. Calcareous nannofossils and Mesozoic oceanic anoxic events. Mar. Micropaleontol. 52, 85–106. doi:10.1016/j.marmicro.2004.04.007.

Erba, E., Tremolada, F., 2004. Nannofossil carbonate fluxes during the early Cretaceous: phytoplankton response to nutrification episodes, atmospheric CO_2, and anoxia. Paleoceanography 19, PA1008 1–18.

Gerlach, T.M., Graeber, E.J., 1985. Volatile budget of Kilauea volcano. Nature 313, 273–277.

Gerlach, T.M., McGee, K.A., Elias, T., Sutton, A.J., Doukas, M.P., 2002. Carbon dioxide emission rate of Kīlauea Volcano: implications for primary magma and the summit reservoir. J. Geophys. Res. B, Solid Earth 107, ECV 3–1-15.

Gradstein, F.M., Agterberg, F.P., Ogg, J.G., Hardenbol, J., van Veen, P., Thierry, J., Huang, Z., 1995. A triassic, jurassic and cretaceous time scale. In: Berggren, W., Hardenbol, J., Kent, D. (Eds.), Geochronology, Time Scales and Global Stratigraphic Correlation. SEPM Special Publication no. 54, pp. 95–126.

Gradstein, F.M., Ogg, J.G., Smith, A.G., Bleeker, W., Lourens, L.J., 2004. A new Geologic Time Scale, with special reference to Precambrian and Neogene. Episodes 27, 83–100.

Gröcke, D.R., 2002. The carbon isotope composition of ancient CO_2 based on higher-plant organic matter. Philos. Trans. R. Soc. Lond. Ser. A: Math. Phys. Sci. 360, 633–658.

Heimhofer, U., Hochuli, P.A., Herrle, J.O., Andersen, N., Weissert, H., 2004. Absence of major vegetation and palaeoatmospheric pCO_2 changes associated with oceanic anoxic event 1a (early Aptian, SE France). Earth Planet. Sci. Lett. 223, 303–318.

Ingall, E., Jahnke, R., 1997. Influence of water-column anoxia on the elemental fractionation of carbon and phosphorus during sediment diagenesis. Mar. Geol. 139, 219–229.

Jahren, A.H., Arens, N.C., Sarmiento, G., Guerrero, J., Amundson, R., 2001. Terrestrial record of methane hydrate dissociation in the early Cretaceous. Geology 29, 159–162.

Jenkyns, H.C., Strasser, A., 1995. Lower Cretaceous oolites from the Mid-Pacific Mountains (Resolution Guyot, Site 866). Proc., Scientific Results, ODP, Leg 143, Northwest Pacific Atolls and Guyots, pp. 111–118.

Kump, L.R., Arthur, M.A., 1999. Interpreting carbon-isotope excursions: carbonates and organic matter. Chem. Geol. 161, 181–198.

Larson, R.L., Erba, E., 1999. Onset of the mid-Cretaceous greenhouse in the Barremian–Aptian: igneous events and the biological, sedimentary, and geochemical responses. Paleoceanography 14, 663–678.

Leavitt, S.W., 1982. Annual volcanic carbon dioxide emission: an estimate from eruption chronologies. Environ. Geol. 4, 15–21.

Leckie, R.M., Bralower, T.J., Cashman, R., 2002. Oceanic anoxic events and plankton evolution: biotic response to tectonic forcing during the mid-Cretaceous. Paleoceanography 17. doi:10.1029/2001PA000623.

Li, Y.-X., Bralower, T.J., Montañez, I.P., Osleger, D.A., Arthur, M.A., Bice, D.M., Herbert, T.D., Erba, E., Premoli Silva, I., 2008. Toward an orbital chronology for the early Aptian Oceanic Anoxic Event (OAE1a, ~120 Ma). Earth Planet. Sci. Lett. 271, 88–100.

Menegatti, A.P., Weissert, H., Brown, R.S., Tyson, R.V., Farrimond, P., Strasser, A., Caron, M., 1998. High-resolution $\delta^{13}C$ stratigraphy through the early Aptian 'Livello Selli' of the Alpine Tethys. Paleoceanography 13, 530–545.

Premoli Silva, I., Erba, E., Salvini, G., Locatelli, C., Verga, D., 1999. Biotic changes in Cretaceous oceanic anoxic events of the Tethys. J. Foraminiferal Res. 29, 352–370.

Price, G.D., 2003. New constraints upon isotope variation during the early Cretaceous (Barremian–Cenomanian) from the Pacific Ocean. Geol. Mag. 140, 513–522.

Redfield, A.C., Ketchum, B.H., Richards, F.A., 1963. The influence of organisms on the composition of sea water. In: Hill, M.N. (Ed.), The Sea, vol. 2. Wiley Interscience, New York, pp. 26–77.

Saal, A.E., Hauri, E.H., Langmuir, C.H., Perfit, M.R., 2002. Vapour undersaturation in primitive mid-ocean-ridge basalt and the volatile content of Earth's upper mantle. Nature 419, 451–455.

Schlanger, S.O., Jenkyns, H.C., 1976. Cretaceous oceanic anoxic events: causes and consequences. Geol. Mijnb. 55, 179–184.

Scholle, P.A., Arthur, M.A., 1980. Carbon isotope fluctuations in Cretaceous pelagic limestones: potential stratigraphic and petroleum exploration tool. AAPG Bull. 64, 67–87.

Stouffer, R.J., Manabe, S., 2003. Equilibrium response of thermohaline circulation to large changes in atmospheric CO_2 concentration. Clim. Dyn. 20, 759–773.

Tajika, E., 1998. Climate change during the last 150 million years: reconstruction from a carbon cycle model. Earth Planet. Sci. Lett. 160, 695–707.

Tajika, E., 1999. Carbon cycle and climate change during the Cretaceous inferred from a biogeochemical carbon cycle model. Isl. Arc 8 (2), 293–303.

Tarduno, J.A., Sliter, W.V., Kroenke, L., Leckie, M., Mayer, H., Mahoney, J.J., Musgrave, R., Storey, M., Winterer, E.L., 1991. Rapid formation of Ontong Java Plateau by aptian mantle plume volcanism. Science 254, 399–403.

Tsujino, H., Hasumi, H., Suginohara, N., 2000. Deep Pacific circulation controlled by vertical diffusivity at the lower thermocline depths. J. Phys. Oceanogr. 30, 2853–2865.

van Breugel, Y., Schouten, S., Tsikos, H., Erba, E., Price, G.D., Damsté, J.S.S., 2007. Synchronous negative carbon isotope shifts in marine and terrestrial biomarkers at the onset of the early Aptian oceanic anoxic event 1a: evidence for the release of 13C-depleted carbon into the atmosphere. Paleoceanography 22, PA1210. doi:10.1029/2006PA001341.

Walker, J.C.G., Hays, P.B., Kasting, J.F., 1981. A negative feedback mechanism for the long-term stabilization of Earth's surface temperature. J. Geophys. Res. 86, 9776–9782.

Weissert, H., Lini, A., Föllmi, K.B., Kuhn, O., 1998. Correlation of early Cretaceous carbon isotope stratigraphy and platform drowning events: a possible link? Palaeogeogr. Palaeoclimatol. Palaeoecol. 137, 189–203.

Yamanaka, Y., Tajika, E., 1996. The role of the vertical fluxes of particulate organic matter and calcite in the oceanic carbon cycle: studies using an ocean biogeochemical general circulation model. Glob. Biogeochem. Cycles 10, 361–382.